# Unraveling lung cancer drivers:

Generation of murine lung organoids to examine LUAD driver mutations

## Minor research project

Heleen Dorothea Jüngen – 6783317
Utrecht University – MSc Cancer, Stem cells, and Developmental Biology
September 2024

Supervisors: Dr. Talya Dayton and Dr. Ana Janic
Dayton lab, EMBL Barcelona
Janic lab, UPF

## Layman's summary

Lung adenocarcinoma is the most common cause of cancer deaths around the world, and only 19% of people with this cancer survive over a long period of time. This type of lung cancer is especially dangerous because of changes, called mutations, in certain genes like *Kras* and *TP53*. These mutations make the cancer grow, spread, and resistant to cancer therapies. Scientists use 3D models called organoids to study this type of lung cancer. These organoids act like mini organs or tumors that help us to see how healthy tissue behaves, and how cancer cells grow and interact with their surroundings. In this research, we are creating healthy lung organoids of mice and several organoid models of lung cancer to understand the role of the *TP53* gene and other important genes in how the cancer progresses from early to late stages. We will use lung cells from healthy mice and cancerous lung cells that have a common mutation in *Kras*, with and without changes in *TP53*. We will also grow these organoids in the presence of different growth factors to see if the tumors are depended on certain factors to grow and stay alive. Additionally, we will develop a special tool to track the specific cell types in the organoids and monitor changes during this study.

## Abstract

Lung adenocarcinoma (LUAD) is the leading cause of cancer-related deaths worldwide, with a survival rate of just 19%. LUAD's aggressiveness is driven by key mutations, particularly in *Kras* and *TP53*. KRAS mutations are found in 10%–30% of LUAD cases, while *TP53* loss-of-function mutations occur in 50%–70%, frequently co-occurring with *Kras* mutations. Organoids, three-dimensional in vitro models that replicate the cellular environment and interactions seen in patient tumors, serve as a powerful system to study tumor progression. This research aims to develop healthy murine lung organoids and multiple LUAD organoid models to investigate the role of P53 and target genes in LUAD progression, from early to late stages. Specifically, organoids will be derived from healthy mouse lungs and murine LUAD cells harboring a $Kras^{G12D}$ mutation, with and without *TP53* loss. Additionally, varying growth factor combinations in the culture media will be used to gain insights into microenvironmental factors that support LUAD growth at different disease stages. A Cas9-EGFP construct will also be generated to facilitate the creation of reporter organoid lines.

# Unraveling lung cancer drivers: generation of murine lung organoids to examine LUAD driver mutations

## Graphical abstract

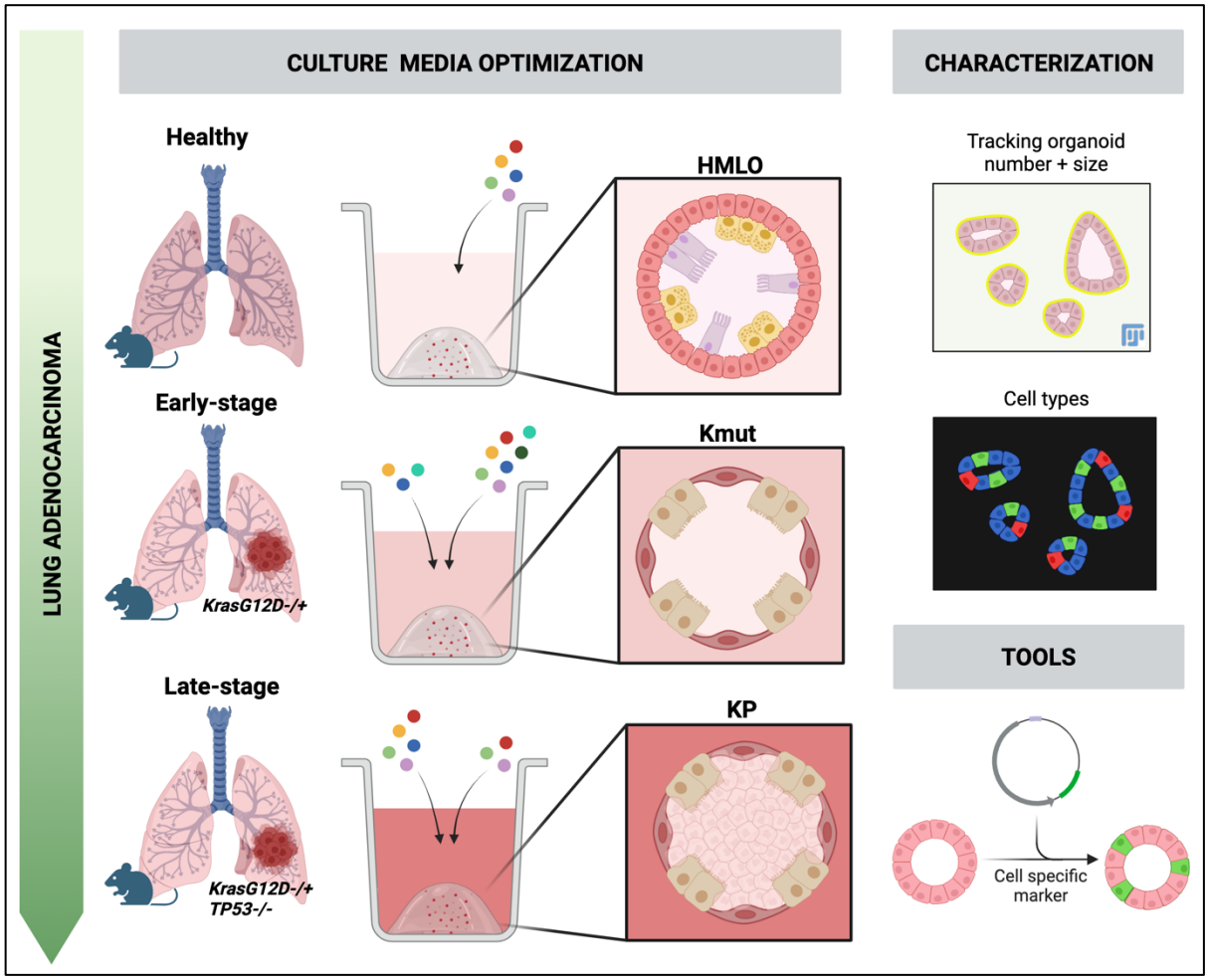

## Introduction

Lung adenocarcinoma (LUAD) is the most common subtype of lung cancer, accounting for 50% of all cases[1]. Due to its aggressive nature and late-stage detection, LUAD leads to the highest number of cancer-related deaths, with an overall survival rate of 19%[2,3]. The incidence of LUAD has been rising, attributed to increased smoking or other non-smoking related factors such as environmental pollution and second-hand tobacco smoke[3]. LUAD typically arises in the peripheral lung or at distal regions of the lung, more specifically in the alveolar regions. In these alveolar regions, alveolar type 1 (AT1) cells are responsible for regulating gas exchange, while alveolar type 2 (AT2) cells produce surfactant protein to decrease alveolar tension during respiration[4]. While AT2 cells were initially identified as the cells of origin for LUAD, recent studies suggest that other cell types can also contribute to its development[5,6].

Large-scale genomic studies have provided significant insights into the mutations driving LUAD development. These driver mutations, found in genes such as *ALK*, *EGFR*, *BRAF*, *TP53*, and *Kras*, typically occur in the lung periphery at sites of scarring and chronic inflammation and are associated with aggressive tumor progression and chemoresistance[7,8]. The most prevalent mutation in LUAD is in *Kras*, which is mutated in 10%-30% of all LUAD tumors[9]. The presence of only a KRAS mutation in LUAD is linked to the early stages of disease development and serves as indicators of the transition from healthy to malignant states[10]. The KRAS protein is active when it is bound to GTP, facilitated by GTPase-activating proteins (GAPs), and inactive when it is bound to GDP, mediated by Guanine nucleotide exchange factors (GEFs) (**Figure 1**)[11]. Additionally, *Kras* acts upstream in the RAF/MEK/MAPK pathway and other pathways such as PI3K-AKT-mTOR[12]. Mutations in the *Kras* gene result in alterations in its GTPase domain, causing reduced sensitivity to upstream signals and constitutive activation[13]. The constitutively active KRAS leads to the overactivation of pathways promoting cell growth, cell survival, and proliferation, contributing to cancer development.

Next to *Kras* mutations, *TP53* loss-of-function mutations are present in about 50–70% of the LUAD cases, co-occurring with *Kras* mutations in approximately 40% of instances[14,15]. The *TP53* gene encodes for a transcription factor regulating over 500 target genes, controlling processes such as the cell cycle, DNA repair, senescence, and cell death[16]. Wild-type *TP53* can induce apoptosis in a transcription independent manner and a transcription dependent manner. In both cases, dimerization of BAX proteins on the mitochondrial outer membrane results in the release of cytochrome C, activating caspases that initiate apoptosis (**Figure 2**)[17]. A well described target gene of *TP53* is *P21*, which, upon transcription, inhibits multiple transitions of the cell cycle, causing cell cycle arrest and enabling DNA repair. However, this arrest can also induce cellular senescence[18]. Loss of *TP53* results in the loss of tumor suppression functions, leading to unregulated cell cycle progression and increased genomic instability[15].

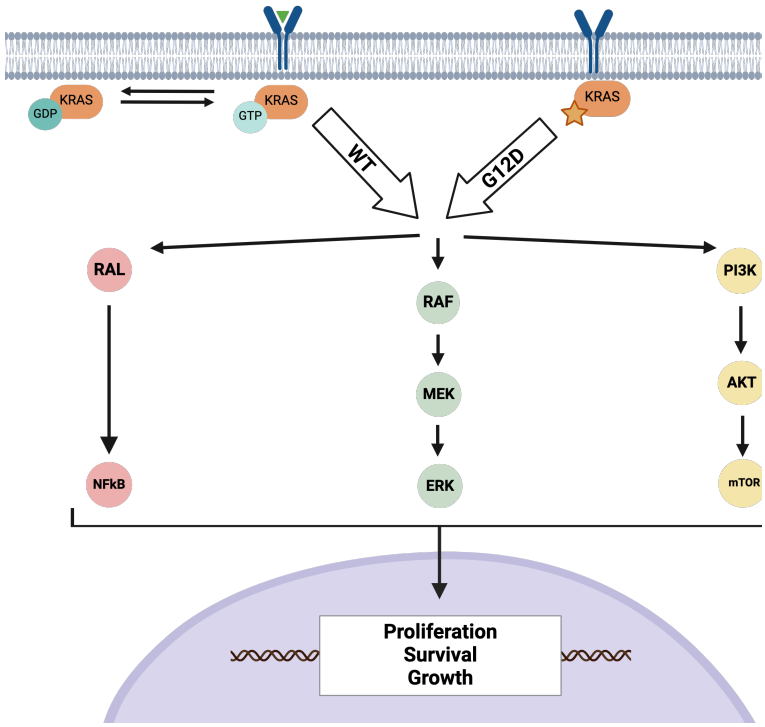


***Figure 1 Activation of the downstream pathways of Kras*** *In the wild-type (WT) situation (left), activated KRAS is bound GTP and subsequently activated its downstream pathways to promote proliferation, cell survival, and cell growth. These downstream pathways can also be activated a mutation in the GTP binding site of KRAS (right).*

Over the past decades, various models have been utilized to investigate LUAD disease progression. Together with tumor cell lines, and patient-derived tumor xenografts, genetically engineered mouse models (GEMMs) have significantly contributed to LUAD research[8]. For instance, the *LSL-Kras*$^{G12D/+}$ and the *LSL-Kras*$^{G12D/+}$*;Tp53*$^{F/F}$ mouse models enable researchers to induce tumor formation via Cre administration to the lung. This leads to activation of oncogenic Kras alone or in combination with loss of *Tp53*, respectively[19–22]. GEMMs offer several advantages over cell lines, such as allowing spontaneous tumor development in an immunocompetent host, modeling specific human cancer mutations, enabling tumor-immune interactions, and facilitating metastasis studies[23,24]. However, GEMMs also have disadvantages, including the use of animals and differences in physiology, genetics, and metabolism between mice and humans, which limit their ability to fully replicate human tumors. Additionally, mouse models are labor-intensive, costly, and time-consuming[25]. Advancements in organoid technology are addressing these limitations by providing more accurate in vitro models that mimic human tumor biology, enhancing the relevance of preclinical cancer research. Organoids, derived from stem cells, are able to self-organize and represent robust three-dimensional in vitro systems that closely resemble their tissue of origin and serve as a suitable model for drug sensitivity of patients[26]. These stem cells can, for example, be sourced from healthy cells to generate healthy tissue organoids or from cancer cells, resulting in the formation of tumor organoids. The cultures of organoids rely on a growth media with a defined composition of small molecules and growth factors[27]. This media was first defined for colorectal cancer organoids and has since then been adapted for other organoid types according to their specific niche requirements for the long-term cell growth[26,27].

Several laboratories have established human and murine lung cancer organoids bearing various mutations[10,28–31]. For example, Dost and colleagues compared organoid models of early-stage LUAD with *Kras*$^{G12D}$ mutations to later-stage LUAD tumors with *TP53* mutation or loss, accurately modeling LUAD progression in vitro[10]. In this research, organoids were co-cultured with stromal cells in an air-liquid interface (ALI) where the stromal cells provide growth signals, eliminating the need for growth factor-defined media. While groups have cultured LUAD organoids with a *Kras*$^{G12D}$ mutation alone or with an additional *TP53* loss (KP), the culture methods have not been standardized, and the media compositions vary, often based on the growth factor cocktails described for colorectal cancer organoids. Additionally, no Kras$^{G12D}$ (Kmut) LUAD cells have been successfully cultured without feeder cells, underscoring the current gap in understanding the signaling dependencies of these cells. As previously noted, media compositions reflect the specific dependencies of tumors for the

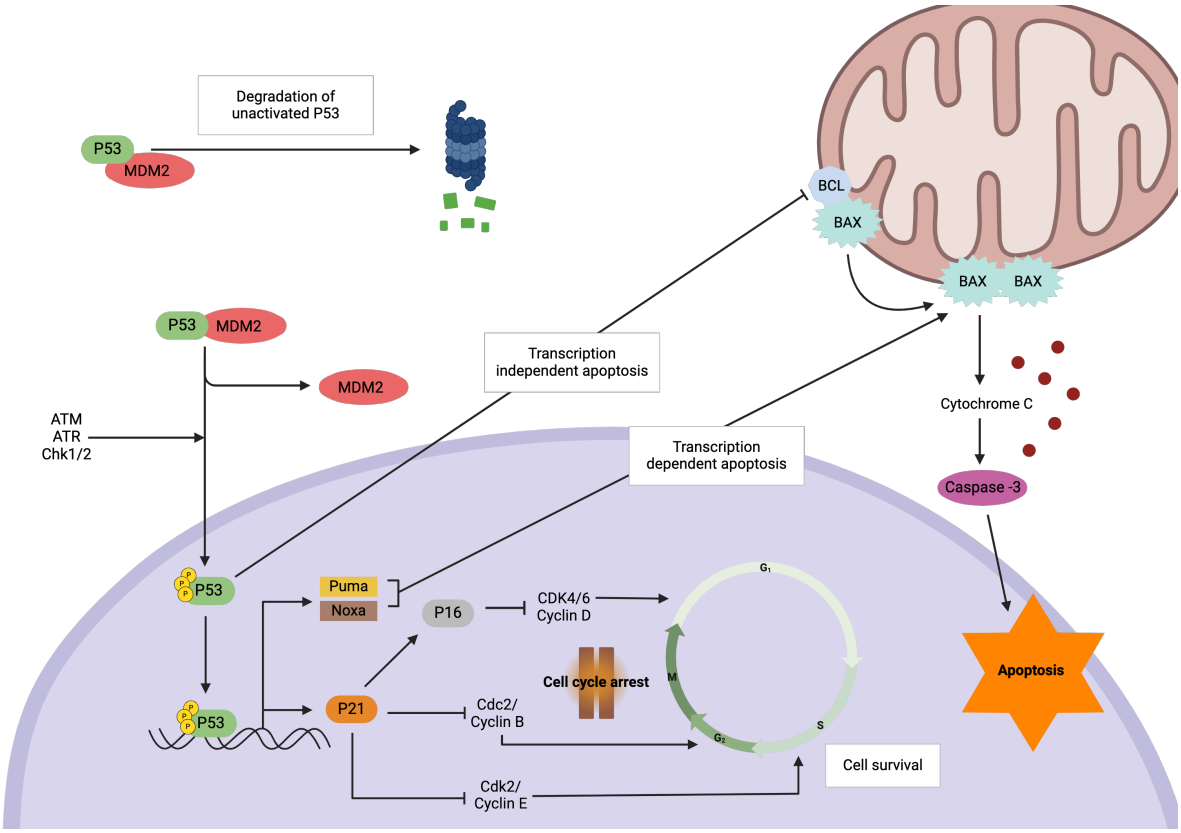


***Figure 2 The p53 signaling pathway mediating cell cycle arrest and apoptosis.*** *A schematic illustrating how activated p53 promotes cell cycle arrest and apoptosis. Activated p53 induces cell cycle arrest by transcribing P21, which inhibits cyclin/CDK complexes, halting cell cycle progression. Simultaneously, p53 promotes apoptosis through transcription of pro-apoptotic genes PUMA and NOXA, and by directly interacting with proteins like BAX to trigger mitochondrial permeabilization and caspase-3 activation. Without activation, P53 is translocated to the proteasome where it is degraded.*

long-term expansion of organoids. This is exemplified by a study from Dayton and colleagues, which demonstrated that patient-derived lung organoids of neuroendocrine neoplasms rely on epidermal growth factor (EGF) for growth[32]. Further research into the media composition of Kmut organoids could uncover the growth dependencies of early-stage LUAD tumors.

In this research, we aim to develop multiple healthy and LUAD murine lung organoid models to test the feasibility of genetically engineering *TP53* and its target genes that have tumor suppression role in LUAD progression and initiation by the clustered regularly interspaced short palindromic repeats (CRISPR)-Cas9 system. More specifically, organoids will be generated from murine LUAD cells bearing a $Kras^{G12D}$ mutation, with and without loss of *TP53* and from lung epithelial cells isolated from a wild-type C57BL/6 mouse with an unaltered genetic background. Different combinations of growth factors in media to maintain the lung cancer organoids aim to provide comprehensive insights into the microenvironment-derived factors that support LUAD growth at different stages of disease progression. Additionally, we generate a Cas9-EGFP construct to enable the establishment of reporter organoid lines.

## Materials and Methods

*Statistical analysis*

Statistical analysis was not conducted due to insufficient sample size, which prevented robust statistical evaluation.

*Mice*

For the generation of healthy murine lung organoids female C57BL/6 mice of 10 weeks old were used. The animal experiment adhered to ethical guidelines for animal research and were conducted with the approval of the Ethics Committee for Animal Experiments (CEEA-PRBB, Barcelona, Spain). Resection of the lungs was performed by Ivan Zadra (Janic lab, UPF).

*Organoid culture and passage*

Cell pellets from healthy mouse lungs, cell lines, or PDX tumors were suspended in 12.5% wash medium consisting of Advanced DMEM/F12 (Gibco, 12634028) supplemented with 1X Glutamax (Gibco, 11574466), 10 mM Hepes (Gibco, 11560496), and 10 mM Pen/Strep (Thermo Fisher Scientific, 15140122). Then, 87.5% basement membrane extract (BME) (R&D systems, 3553-101-02) was added. A 40 µL droplet of the BME-cell mixture was placed into each well of a pre-warmed 24-well plate (Falcon) and incubated at 37°C with 5% CO2 for 30 minutes to allow the BME droplets to solidify. After solidification, 1 mL of culture medium was added to each well, and the cells were incubated at 37°C with 5% CO2. Different media formulations were used based on the experimental condition (**Table S1**). Media was refreshed weekly in all conditions. Organoids were regularly monitored and passaged either weekly or biweekly, depending on their growth rate. For passaging, organoids were collected with 1 mL of TripleE (Thermo Fisher Scientific, 12605028) and incubated at 37°C for 2 minutes. Then, the organoids were dissociated into single cells by pipetting the suspension up and down with a 5 mL pipette fitted with a 10 µL pipette tip, and 5 mL of wash medium was added. The single cells were centrifuged at 1500 rpm for 5 minutes at 12°C. After the supernatant was removed, the cells were resuspended in BME and replated following the same procedure previously described.

*Tissue processing and preparation of murine lung organoids*

Lungs from a female 10-week-old C57BL/6 mouse were surgically removed and immediately placed in PBS for same-day processing. The lungs were finely chopped with a scalpel and washed in 4 mL wash media. To break down the tissue, an enzymatic digestion was performed using 2 mg/mL collagenase (MERCK, C9407) in wash media, with the mixture incubated on a rotating shaker at 37°C for 2 hours. Once digested, the tissue was further dissociated by pipetting the suspension repeatedly with a 10 mL pipette. The resulting cell suspension was passed through a 100 µm filter, and tissue fragments trapped in the filter were mechanically broken down by pressing them with the back of a syringe plunger before re-filtering along with the supernatant. Centrifugation was performed at 1200 rpm, and the supernatant was discarded. After washing the cell pellet in wash media, the cells were centrifuged again at 1200 rpm. To eliminate erythrocytes, the cell pellet was resuspended in 2 mL of red blood cell lysis buffer (Sigma, 11814389001) and incubated for 5 minutes at room temperature. The lysis was terminated by adding 5 mL of wash media, followed by another round of centrifugation. Finally, cells were resuspended in BME and plated to promote the growth of healthy mouse lung organoids.

*DNA extraction from organoid cells*

To obtain DNA from the organoids, a small cell pellet was collected during passaging and centrifuged. After centrifugation, the supernatant was removed, and the cell pellet was stored at -20°C until further use. For DNA isolation, the cell pellet was thawed and centrifuged at 1500 rpm for 5 minutes at 4°C. Once the remaining media was removed, a portion of the cell pellet was transferred to a 1.5 mL Eppendorf tube using a 200 µL pipette tip. Then, 75 µL of Alkaline lysis buffer, consisting of 10N NaOH, 0.5M EDTA, and distilled water, was added to the tube. The mixture was incubated at 95°C for 95 minutes to lyse the cells. After incubation, the sample was cooled at 4°C for 15 minutes, and 75 µL of Neutralization buffer, containing 6.3 mg/mL Tris-HCl and distilled water, was added to neutralize the reaction. The DNA concentration was measured using the Nanodrop 200c (Thermo Fisher), and the sample was stored at -20°C for future use.

*Characterization of the $KRAS^{G1D2/+}$ ; $TP53^{-/-}$ genotype in KP organoids*

To verify the presence of the $Kras^{G12D}$ mutation and *TP53* loss in our organoids, a polymerase chain reaction (PCR) was conducted using DNA isolated from KP92 organoids and DNA extracted from a wild-type old C57BL/6 mouse ear tip as a control. The primers used were previously described by the Jacks lab (MIT, Boston).

*TP53A: 5'-CACAAAAACAGGTTAAACCCAG-3'*
*TP53B: 5'-AGCACATAGGAGGCAGAGAC-3'*
*TP53D: 5'-GAAGACAGAAAAGGGGAGGG-3'*
*Kras1: 5'-GTCTTTCCCCAGCACAGTGC-3'*
*Kras2: 5'-CTCTTGCCTACGCCACCAGCT-3'*
*Kras3: 5'-AGCTAGCCACCATGGCTTGAGTAAGTCTGCA-3'*

The PCR reaction mixture for *TP53* amplification was prepared in a total volume of 10 µL and contained 1.0 µL of DNA, 0.5 µL of primer A (10 µM), 0.25 µL of primer B (10 µM), 1 µL of primer D (10 µM), 2.25 µL of Milli-Q water, and 5.0 µL of GoTaq Green Master Mix (Promega, M5123). The PCR reaction mixture of *Kras* with a total volume of 10 µL contained 1.0 µL of DNA, 0.5 µL of primer 1 (10 µM), 0.5 µL of primer 2 (10 µM), 0.5 µL of primer 3 (10 µM), 2.5 µL of Milli-Q water, and 5.0 µL of GoTaq Green Master Mix .The same PCR program was used to amplify both genomic regions starting with the initial denaturation at 95°C for 2 minutes, followed by 34 cycles of denaturation at 94°C for 30 seconds, annealing at 61°C for 30 seconds, and extension at 72°C for 45 seconds, with a final extension at 72°C for 10 minutes.

*Nutlin treatment of KP92 organoids*

KP92 organoids were cultured and passaged following standard protocols. During plating, organoids were seeded into a 24-well plate (Falcon), with three wells assigned to the Nutlin treatment group (Medchemexpress, 10193952) and three wells reserved as controls. Nutlin was added to the treatment group at a final concentration of 10 µM, while the control group remained untreated. The organoids were incubated for 9 days under standard culture conditions, allowing them to reach full maturity. After the treatment period, the presence and phenotype of the organoids were evaluated using microscopy and compared between the Nutlin-treated and untreated control groups.

*KP92 media optimization and image analysis*

To optimize the culture medium for organoid growth, 20 different media formulations were developed and tested (**Table S1**). For each condition, 4500 cells were seeded per well in a 48-well plate (Falcon), with each condition plated in triplicate. Organoids were cultured for 3 weeks, with media being refreshed weekly. Weekly images of the organoids were captured using an EVOS microscope equipped with a 2x objective lens. A single image was taken per well, aiming to capture the entire well in each shot. Image analysis was performed using FIJI (ImageJ) software, where a custom macro was applied to segment the organoids. Manual adjustments were made to account for any 2D structures in the background. The size of single cells on the first day post-plating was used to establish a threshold, ensuring proper differentiation between organoids and individual cells for accurate analysis. Organoids located at the image borders were excluded. After segmentation, the number and size of the organoids were quantified and analyzed to evaluate the effects of the different media formulations. Wells in which the BME drop distanced from the bottom of the well, including all drops from M19, were excluded from the analysis.

*Immunofluorescence of organoids*

HMLOs and KP91 organoids were harvested using fresh wash media. Following centrifugation, the media was removed, and the organoid pellet was washed twice with phosphate-buffered saline (PBS). The washed organoids were subsequently treated with 1 mL of 4% paraformaldehyde (PFA) for 10 minutes at 4°C. After an additional centrifugation step, the

organoids were stored in PBS overnight at 4°C. On the following day, organoids were permeabilized using 0.3% Triton X-100 in PBS for 10 minutes at room temperature. After permeabilization, blocking was performed with 6% bovine serum albumin (BSA) and 0.1% Triton X-100 in PBS for 1 hour at RT. The organoids were incubated overnight at 4°C with the primary antibodies anti-TTF1 (Abcam, ab76013) and p53 (DO-1) (Santa Cruz Biotechnology, sc-126). The following day, organoids were washed three times with PBS for 5 minutes each and incubated with the secondary antibodies donkey anti-rabbit IgG Alexa Fluor™ Plus 488 (Thermo Fisher, A32790), donkey anti-mouse IgG Alexa Fluor™ Plus 555 (Thermo Fisher, A32773), along with DAPI and Phalloidin (Thermo Fisher, A22287) in blocking solution for 1 hour at room temperature. Organoids were then washed twice with PBS for 5 minutes. The organoids were mounted on glass 6-well chamber slides using Fluoroshield (without DAPI). Imaging was performed using the Viventis LS1 microscope, and image processing was conducted using FIJI software.

*Plasmid design and construction*

The EF1a-Cas9-EFGP-Puro plasmid was designed using MacVector software, utilizing the lenti-Cas9-2A-EGFP-vMC+PGK_BSD_B plasmid (**Figure S1**) as the backbone for the final construct. The EF1a-Cas9-2A-EGFP sequence was isolated from this plasmid using the following primers:

*Forward: 5'-CCCGCAAGCCCGGTGCCTGAGAGGATCCCTGATGTGCCTT-3'*

*Reverse: 5'-GGGCGATGTGCGCTCTGCCCGGGTGAGATAACTTCGTATAAGG-3'*

To achieve a high DNA yield after isolation from the agarose gel, 10 PCR reactions were performed for the amplification of the EF1a-Cas9-2A-EGFP sequence. Additionally, the EF1a-Puro insert was amplified from the 1926-Seq1-Tol2-ppGk-mCh-NLS-pA-pEFS-puro-pA-Tol2 plasmid (**Figure S2**) using the following primers:

*Forward: 5'-TATACGAAGTTATCTCACCCGGGCAGAGCGCACATCGCCC-3'*

*Reverse: 5'-AAGGCACATCAGGGATCCTCTCAGGCACCGGGCTTGCGGG-3'*

The amplified DNA fragments were separated by 1% agarose gel electrophoresis, followed by DNA extraction using the GeneJET Gel Extraction Kit (Thermo Fisher, 2919786). The isolated fragments were then ligated with the GeneArt Gibson Assembly HiFi Cloning Kit (Thermo Fisher, A46629) according to the manufacturer's instructions. The ligation product was transformed into Stbl3 competent cells (Fisher Scientific, 10193952) for bacterial expansion and a plasmid Maxi Prep was conducted using the EndoFree Plasmid Maxi Kit (Qiagen, 12362) to obtain a high-yield plasmid preparation. Sequencing of the final EF1a-Cas9-EFGP-Puro plasmid was carried out by Plasmidsaurus to confirm successful construction (**Figure S3**).

## Results

### Generation and morphological characterization of healthy murine lung organoids

To facilitate CRISPR-based genetic manipulation of specific tumor suppressors in this model, healthy murine lung organoids (HMLOs) were generated. Healthy lungs from a female 10-week-old wild-type C57BL/6 mouse were excised and enzymatically dissociated to obtain a single-cell suspension, which was then cultured in a medium previously used for human lung organoids (**Table S1**)[30]. Half of the cell suspension underwent fibroblast depletion before plating (**Figure 3A**). After one week, HMLOs developed from both cell suspensions, with or without fibroblast depletion, forming polarized structures with a clear outer border and a distinct inner mass containing single cells (**Figure 3B**). Following passage, new organoids reached full maturity after two weeks (**Figure 3B**). Long-term cultures of fibroblast-depleted organoids exhibited homogeneous morphology, while cultures without fibroblast depletion showed a diverse range of organoid morphologies, from polarized structures to more solid structures with branching edges (**Figure 3C**). Moreover, a novel spherical phenotype appeared across multiple wells (**Figure 3C**).

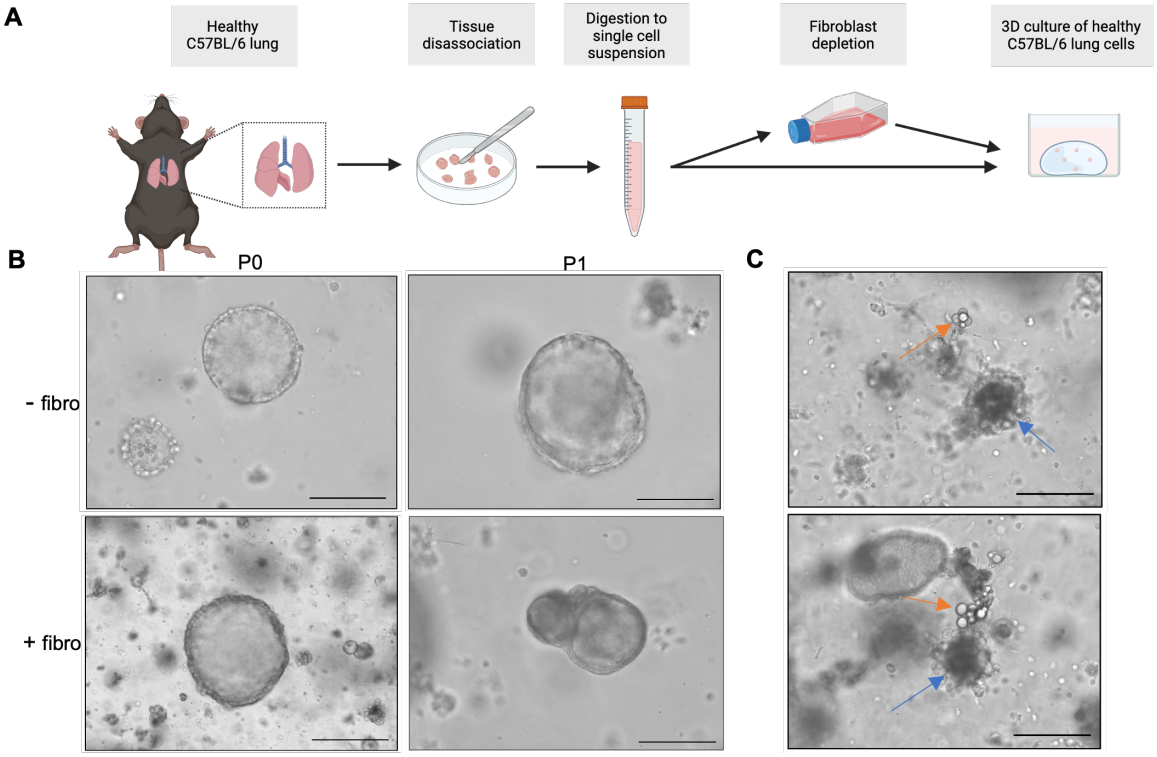


***Figure 3 Isolation and 3D culture of lung cells from WT C57BL/6 mice A)*** *Schematic representation of the steps involved in processing the lung tissue, from disassociation to 3D culture.* ***B)*** *Representative phase-contrast microscopy images show HMLOs one week after seeding stages of culture (P0, left) and after the first passage (P1, right). Organoids where cultured with fibroblast depletion (- fibro) and without fibroblast depletion (+ fibro).* ***C)*** *Representative phase-contrast microscopy images of heterogenous organoid growth showing a spherical phenotype (orange arrows) and branching phenotypes (blue arrows). Scale bars represent 150 µm.*

**Optimization of feeder-free culture conditions for *Kras$^{G12D/+}$* lung adenocarcinoma organoids**

To establish optimal feeder-free conditions for the propagation of *Kras$^{G12D/+}$* (Kmut) lung adenocarcinoma cells, murine Kmut lung tumor cells isolated from mouse LUAD tissue were cultured in healthy lung media supplemented with either B27 or Insulin, Transferrin, Selenium (ITS) (**Table S1**). In a parallel experiment, Wnt3a was included to enhance Wnt signaling, SB202190 was excluded to maintain active P38 mitogen-activated protein kinase (MAPK), and epidermal growth factor (EGF) was added to promote proliferation (**Table S1**). Culturing Kmut

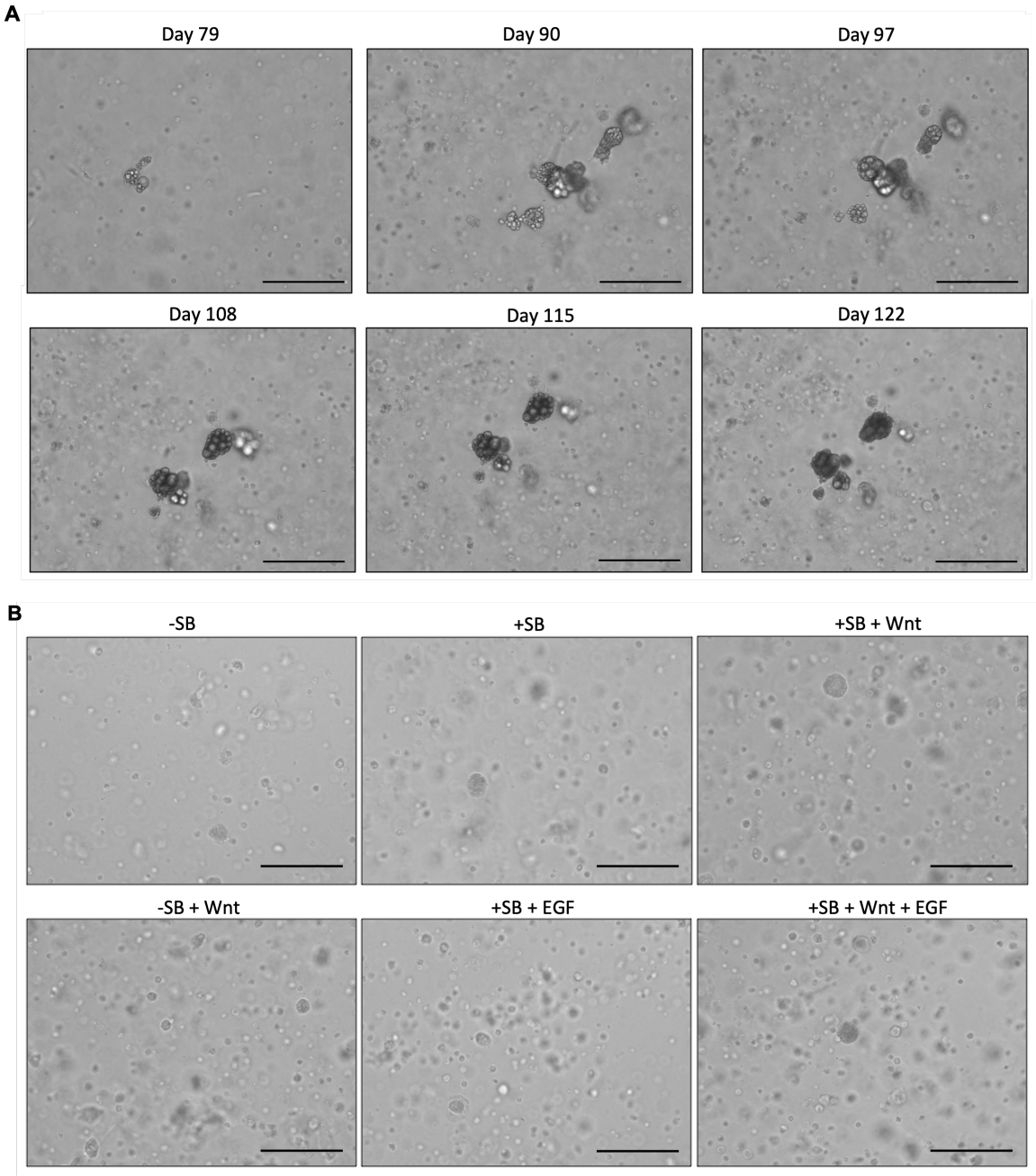


***Figure 4 Time-lapse and optimization of culture conditions for Kmut cells to promote organoid formation*** *Representative phase-contrast microscopy images illustrating* ***A)*** *The formation of Kmut cell spherical colonies in an organoid culture system from day 79 to day 12.* ***B)*** *KMUT lung cell cultures subjected to various culture conditions aimed at mimicking the natural microenvironment. Conditions include the presence or absence of the TGF-β inhibitor SB431542 (-SB/+SB), Wnt, and EGF. Scale bars represents 150 μm.*

cells in healthy lung media supplemented with either B27 or ITS facilitated the gradual formation of organoid-like cell clusters in both conditions. However, no substantial organoid expansion was observed (**Figure 4A**). After two months, spherical structures emerged, resembling those observed in healthy lung organoids (**Figure 4A, Figure 3C**). These structures progressively branched and increased in size and density. Additionally, culturing Kmut cells in healthy lung media with or without Wnt, SB202190, and EGF, or their various combinations, resulted in the formation of organoid-like cell clusters, yet no mature organoid development was observed under any tested conditions (**Figure 4B**). The cell clusters displayed either a flattened and transparent morphology, or a colony of small dark cells (**Figure S4**). Imaging after a culture period of one month confirmed the absence of organoid maturation (**Figure 4B**).

**Generation and optimization of murine *Kras$^{G12D/+}$;TP53$^{fl/fl}$* lung adenocarcinoma organoids**

To gain a deeper understanding of the advanced stage of LUAD, we sought to generate LUAD organoids harboring the Kras$^{G12D}$ mutation and *TP53* loss. To achieve this, we utilized early passaged cells derived from three Kras$^{G12D/+}$; P53$^{fl/fl}$ tumor bearing mice, hereafter called KP91, KP92, and KP93. These single cells were cultured in BME and maintained in two different media conditions for healthy lung tissue and 2D cell culture in the Janic laboratory (MJ) (**Table S1**)[30].

*Genetic and cellular characterization of HMLOs and KP organoids*

To validate that the generated organoids harbored the *Kras$^{G12D}$* mutation and *TP53* loss, PCR analysis was conducted on DNA from KP92 organoids to detect the recombined *Kras$^{G12D}$* allele and *TP53* deletion (Berns allele) (**Figure 5A**). KP92 samples exhibited both the mutated *Kras* band (622 bp) and the wild-type *Kras* band (650 bp), while the control sample displayed only the wild-type *Kras* band (**Figure 5C**). Furthermore, no wild-type *TP53* band (288 bp) was detected in the KP92 organoids, while the recombined *TP53* deletion band (612 bp) was present (**Figure 5B**). The control sample exclusively showed the wild-type *TP53* band. To further confirm the *TP53* loss, KP92 organoids were treated with Nutlin, an MDM2 inhibitor that activates P53. The outgrowth of organoids exhibiting the same phenotype as the untreated control group confirmed the absence of functional *TP53* (**Figure S5).** To further characterize the cellular composition of the KP91 organoids, immunofluorescence was performed alongside HMLOs. Thyroid Transcription Factor-1 (TTF-1), a marker for alveolar and bronchiolar epithelial cells, was detected in the nuclei of both the KP91 organoids and the HMLOs (**Figure 5D**).

*Optimization KP organoid media*

To establish an optimal culture medium that supports robust organoid growth while maintaining controllable size and preserving cellular diversity, we conducted a screen of essential organoid media components commonly cited in the literature as critical for organoid culture (**Table S1**). Organoid growth was compared between a master mix (MM) containing

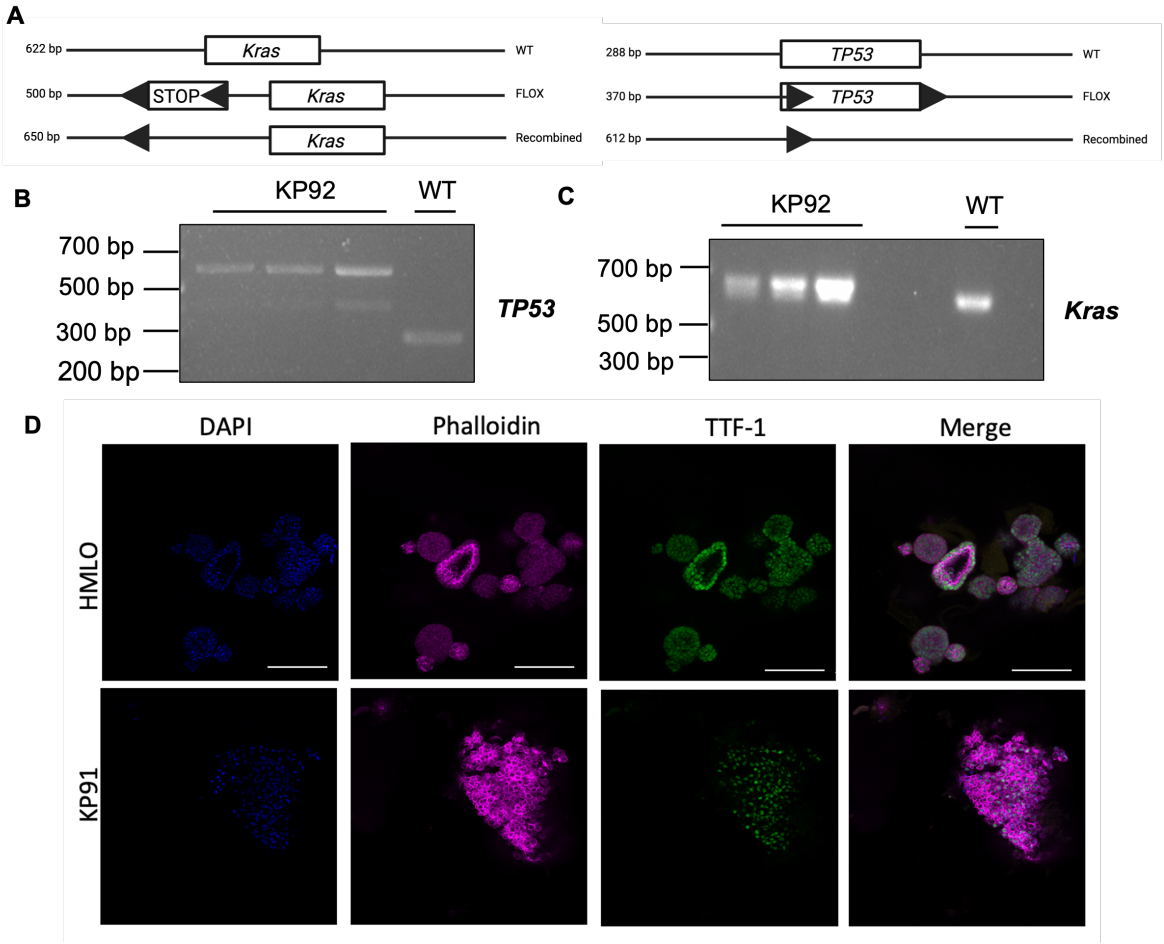


***Figure 5 Genotyping of KP organoids and immunofluorescence staining of KP91 and HMLO organoids. A)*** *Schematic representation of the Kras and TP53 wild type (WT), floxed (FLOX) alleles and their recombined forms and their size in base pairs (bp).* ***B,C)*** *Gel electrophoresis of KP92 organoids containing the recombined Kras (650 bp) and TP53 (612 bp) genes. As a control we used DNA of a wild type C57BL/6 mouse (WT).* ***D)*** *Representative immunofluorescence images of HMLOs and KP91 organoids for nuclear (DAPI in blue), cytoskeletal (Phalloidin in purple), and alveolar/bronchiolar marker (TTF-1 in green). Scale bars represents 320 µm.*

all components and a series of conditions where individual factors were removed from the MM. Additionally, each component was separately added to a basic medium (MB) to evaluate its specific effects. Organoid growth and number were tracked phenotypically over a period of three weeks. In conditions M2, M3, and M6, the organoids consistently showed stable size and number (**Figure 6A**), while in M7 and M8, 2D structures formed without organoid formation (**Figure 6A**). Other conditions produced mixed growth patterns or no growth (**Figure 6A**). The MM condition yielded the highest number of organoids, all of which were relatively uniform in size without cells growing in 2D (**Figure 6A**).

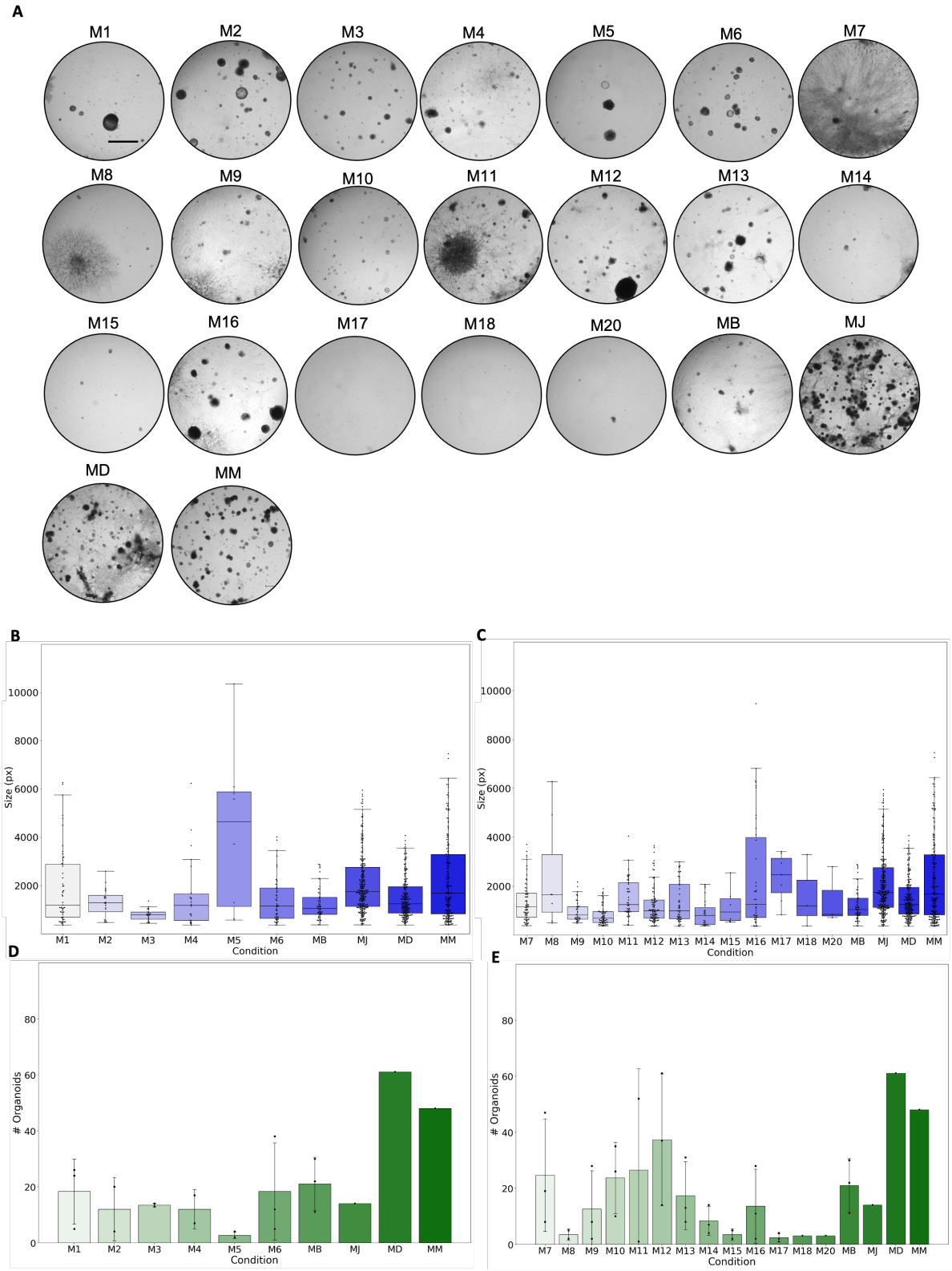


***Figure 6 Assessment of KP92 organoid formation and growth under different media conditions A)*** *Representative bright-field images of organoids formed under various media conditions. Data represent pooled results from three technical replicates. Each dot corresponds to an individual organoid. Scale bar represents 650 uM* ***B/C)*** *Box plot quantifying the average organoid size (in pixels) after two weeks for conditions M1 to M20, MB, MJ, MD, and MM.* ***D/E)*** *Bar graph showing the average number of organoids after two weeks formed per media condition from M1 to M20, MB, MJ, MD, and MM. Each dot represents the average organoid size from one well. Data shown are from three technical replicate. All error bars show the SD.*

Quantitative analysis of organoids growth and number revealed that the exclusion of each component separately from the MM reduced the average organoid size compared to the MM condition, except for the exclusion of Primocin (M5) (**Figure 6A**). Removing Primocin from the medium resulted in a marked increase in organoid size but a decrease in organoid number (**Figure 6D**). Conversely, the addition of individual components, including Noggin, ITS, A8301, R-spondin, and EGF (M9-10, M13-14, M18-20), to the basic medium did not produce organoids of similar size to those in the MM condition (**Figure 6C**). Additionally, none of these factors induced the formation of an organoid number comparable to that observed in the MM condition (**Figure 6E**). Addition of nicotinamide (M8) and FGF7 (M16) to the basic medium increased organoid size to the same size as in the MM condition (**Figure 6C**). Overall, the exclusion of any single component from the MM revealed to disrupt the balance necessary for optimal and consistent organoid growth.

*Dependence of KP organoid growth on growth factors and small molecules*

Organoid counts revealed that the MM condition markedly increased organoid formation compared to both the basic medium (MB) and MB supplemented with Nicotinamide (**Figure 7A**). Removing Nicotinamide from MM led to a substantial decrease in organoid number, while the MB and MB + Nicotinamide conditions produced fewer organoids overall (**Figure 7A**). Similarly, organoid counts in the presence of N-acetylcysteine show that MM led to the highest number of organoids (**Figure 7B**). Excluding N-acetylcysteine from MM resulted in a marked reduction in organoid formation, while the addition of N-acetylcysteine to MB increased organoid number compared to MB alone (**Figure 7B**).

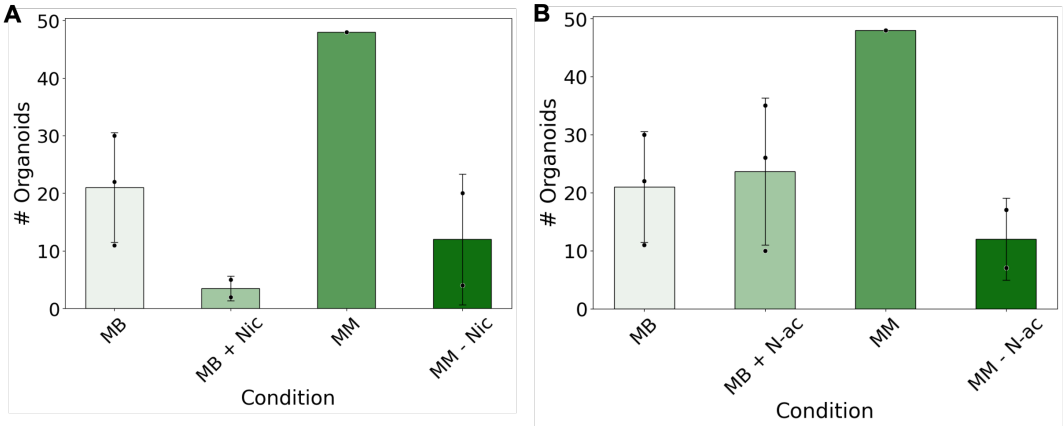


***Figure 7 Organoid formation in media conditions with and without the addition of Nicotinamide or N-acetylcysteine*** *A) Number of organoids per media condition after two weeks, respectively. Conditions include MB, MB + Nicotinamide, MM, and MM - Nicotinamide B) Number of organoids per media condition. Conditions include MB, MB + N-acetylcysteine, MM, and MM – N-acetylcysteine. Each dot represents the average organoid size from one well. Data shown are from three technical replicate. Error bars represent SD.*

**Insertion of Puromycin Resistance in a Cas9-EGFP Vector for Lung Organoid Engineering**

To facilitate the genetic engineering of HMLOs using CRISPR-Cas9 and the generation of a cell reporter line, we aimed to generate a plasmid that would enable constitutive expression of

Cas9 under control of an EF1a promotor, including a puromycin resistance cassette. Leveraging two plasmids we amplified the puromycin resistance cassette from one (insert) and amplified the Cas9-EGFP portion of another (backbone) (**Figure 8A, Figure S1/2**). Gel electrophoresis of the insert and the backbone showed bands consistent with the expected sizes of 818 bp and 13266 bp, respectively (**Figure 8B**). Diagnostic restriction analysis of ligation product revealed band patterns consistent with the anticipated sizes (**Figure 8C/D**). Plasmid sequencing confirmed the successful replacement of the blasticidin cassette with the puromycin cassette (**Figure S3**).

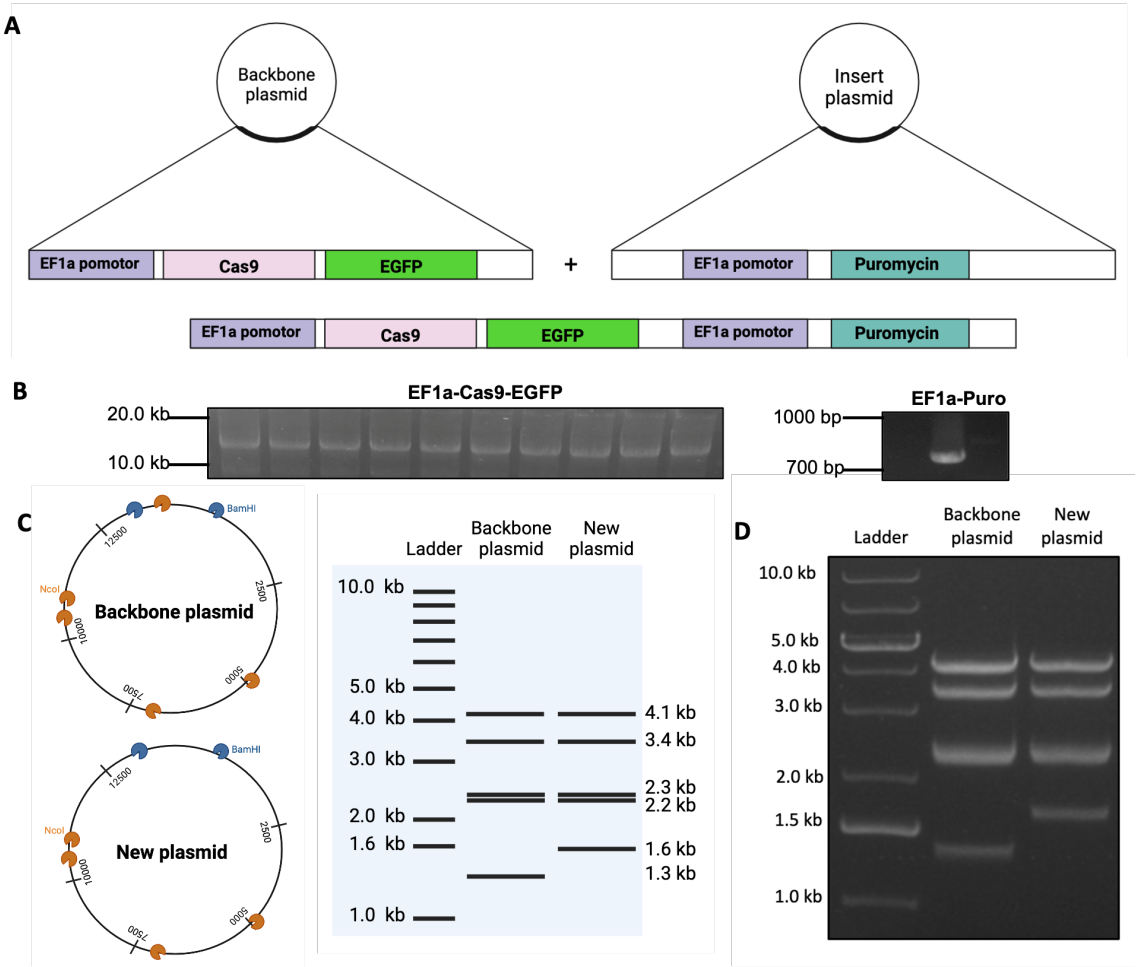


***Figure 8 Construction and verification of a plasmid containing Cas9, EGFP, and puromycin resistance. A)*** *Schematic representation of the plasmid construction in which a backbone plasmid containing the Cas9 and EGFP genes under the control of the EF1α promoter was combined with an insert plasmid containing a puromycin resistance cassette also under the EF1α promoter.* ***B)*** *Image of the gel electrophoresis of PCR reactions of the backbone (EF1a-Cas9-EGFP) fragment and the insert (EF1a-Puro) fragment, respectively.* ***C)*** *Schematic illustration of restriction sites of the backbone and insert plasmid by BamHI and NcoI and expected bans after digestion.* ***D)*** *Image of the gel electrophoresis of a diagnostic digestion of the old backbone plasmid and the new plasmid.*

## Discussion

In this study, we established a variety of murine lung organoid models to study different stages of LUAD progression. We successfully generated HMLOs in a feeder-free system which exhibited polarized structures and demonstrated long-term expansion potential. To model more advanced stages of LUAD, we explored the effects of combining *Kras*$^{G12D}$ mutations with *TP53* loss in murine organoids. Through systematic optimization of the culture medium, we identified critical components necessary for consistent organoid growth and morphology. Finally, to facilitate the study of early-stage LUAD, this feeder-free system was adapted to generate Kmut LUAD organoids. However, Kmut LUAD organoids did not show significant growth in culture and further optimization of the culture conditions is required. The HMLOs and KP LUAD organoids developed in this study are valuable tools for studying LUAD development and progression.

Previous studies have generated HMLOs from either adult lung stem/progenitor cells (AdSCs) or induced pluripotent stem cells (iPSCs), leading to the development of various organoid types depending on the stem cell source[33]. For instance, bronchiolar organoids containing goblet and ciliated cells have been derived from bronchoalveolar stem cells, while alveolar organoids composed of AT1 and AT2 cells can emerge from AT2 cells[33]. Our organoids were generated from the entire murine lung, allowing for the potential outgrowth of diverse AdSC types and the generation of different types of organoids. The observation of multiple morphologies within the same culture, including structures with varying border thickness and branch sites, may reflect these heterogeneous stem cell populations inherent in the murine lung. A study highlighting the importance of fibroblasts in the formation of bronchoalveolar lung organoids (BALOs) observed a similar branching morphology, suggesting that the branching morphologies observed in our heterogeneous culture might be BALOs[34]. Consistent with this, we observe this phenotype more frequently in cultures where fibroblast-like cells have not been depleted, compared to those where these cells have been removed. Further characterization of the fibroblast-like cells we observed are needed to confirm this hypothesis.

The media we tested for the culture of murine Kmut cells did not support the outgrowth of organoids. Previous research demonstrated that P38 MAPK activity, triggered by Wnt signaling, is crucial for intestinal stem cell function[35]. The lack of organoid outgrowth observed with the addition of Wnt, EGF, the absence of the p38 inhibitor, SB202190, or their combinations suggests that the same mechanism is not present in Kmut cells. This aligns with findings showing that P38 inhibition enhances cancer stem cell properties in lung cancer[48]. Additionally, although Wnt/β-catenin pathway activation has been described to stimulate proliferation, inhibit apoptosis, support the maintenance of cancer stem cell populations in lung cancer, and initiate the formation of lung cancer organoids, Wnt supplementation did not increase proliferation in our models[36]. This suggests that the role of Wnt in organoid formation may depend on the tumor stage, with early-stage LUADs relying on different signals for cell proliferation compared to late-stage LUADs. Alternatively, it is possible that the Wnt

concentration was insufficient to establish a Wnt niche for the organoids. Lastly, the lack of response to EGF supports previous studies showing that EGF is supportive but not essential for lung organoid formation[36].

We observed organoids with transparent and flattened morphology in our Kmut cell cultures, which is a typical morphology of senescent cells[37]. Multiple studies have shown that primary rodent cells with hyperactivation of Ras can undergo cell cycle arrest or cellular senescence (Figure 2)[38,39]. We also observed Kmut colonies that had darker morphologies and were difficult to follow over time, which could be indicative of cellular apoptosis. In healthy epithelial cells, elevated Ras activity typically promotes survival and proliferation. However, in transformed cells, Ras activation can paradoxically trigger apoptosis[40]. Based on our results, we cannot conclude whether or not the cells in our culture are undergoing senescence, apoptosis, or both. Future experiments could clarify this by assessing senescence markers such as p16INK4a and p21CIP1 using techniques like quantitative PCR, western blotting, or immunohistochemistry. Additionally, cell death could be evaluated with microscopy by the uptake of DAPI by Kmut cells.

An alternative explanation for the lack of organoid formation could be the absence of appropriate environmental factors in the culture conditions. Previous research has shown that murine Kmut organoids can be successfully generated in co-culture with supportive cells, such as stromal and mesenchymal cells, which is due to the production of cytokines and growth factors that promote tumor proliferation through paracrine signaling[10,41]. Although our culture contained a heterogeneous population of cells, it is likely that the supportive cells creating this niche were not maintained in our culture and that our media conditions did not contain the necessary paracrine factors. For future research IL-6 would be a promising candidate to add to the culture media, since it has been shown to promote stem cell behavior and proliferation in lung cancer cells[42]. Additionally, it has been described that TGF-β can induce proliferation in lung cancer cells[41,43]. In healthy lung organoid media, TGF-β is typically inhibited by Noggin and A8301. Leaving these two components out of the media and adding TGF-β to the culture media could induce cell proliferation. In alveolar organoid cultures co-cultured with mesenchymal cells, no factors are added to inhibit the TGF-β pathway[33]. Another method to identify additional factors could be the analysis of single-cell data from Kmut cells co-cultured with stromal cells, as reported in studies like those by Dost et al. By leveraging NicheNet for ligand activity prediction analysis, we can determine which ligands are most likely to influence gene expression and induce proliferation of our Kmut cells[10,44].

We developed three different murine KP organoid lines; KP91, KP92, and KP93. Testing of different combinations of growth factors in KP growth media revealed potential growth dependencies of KP organoids. For example, organoids proliferate more rapidly in the MM condition including nicotinamide compared to MM alone. Nicotinamide may act as an antioxidant, helping to mitigate ROS-mediated stress. Interestingly, the opposite trend was

observed when nicotinamide was added to the basic media (MB). The low levels of ROS in slow proliferating cells, might explain this observation. This finding aligns with previous research in mice showing that nicotinamide significantly decreases the size of low-grade adenomas, but not of more proliferative LUADs[45]. Addition of N-acetylcysteine to either MM or MB significantly enhanced organoid formation. This finding is in line with earlier research showing that continuous treatment with N-acetylcysteine can promote and stimulate progression of lung cancer in mice[46,47]. Overall, these findings underscore the promoting effect of antioxidants on the progression of LUAD.

Thyroid transcription factor 1 (TTF-1) is a marker for alveolar and bronchial cell types and also broadly used in clinics to identify LUADs[48]. TTF-1 was present both in our HMLOs and KP91 organoids confirming the presence of alveolar and bronchiolar cell types in our organoids. However, future experiments could focus on more in detail characterization of both HMLOs and KP organoids. This is of importance to determine whether our organoids mimic the tissue of origin. In future work we will check for more specific markers such Surfactant Protein C (Sfpc) as for AT2 cells or Advanced Glycosylation End-Product Specific Receptor (AGER) for AT1 cells by immunofluorescence or immunohistochemistry[49]. Identifying the cell types in our culture will also give us information about the effect of our established media on the differentiation potential in our organoids, since it is known that different media ingredients can push the differentiation of stem cells toward specific cell fates[33].

Even though we did not characterize all cell types of our organoids in detail, the phenotypes present in our organoid culture align with morphologies described in earlier studies. Therefore, we conclude that our organoids function as a solid foundation to study the role of different cancer mutations in LUAD progression. The established Cas9-EGFP-Puro construct will help to test this in our healthy and KP organoids.

## References


1. Bray, F. *et al.* Global cancer statistics 2018: GLOBOCAN estimates of incidence and mortality worldwide for 36 cancers in 185 countries. *CA. Cancer J. Clin.* **68**, 394–424 (2018).
2. Wu, B. *et al.* Prognostic factors and survival prediction for patients with metastatic lung adenocarcinoma: A population-based study. *Medicine (Baltimore).* **101**, e32217 (2022).
3. Succony, L., Rassl, D., Barker, A., McCaughan, F. & Rintoul, R. Adenocarcinoma spectrum lesions of the lung: Detection, pathology and treatment strategies. *Cancer Treat. Rev.* **99**, 102237 (2021).
4. Liberti, D. C. & Morrisey, E. E. Organoid models: assessing lung cell fate decisions and disease responses. *Trends Mol. Med.* **27**, 1159–1174 (2021).
5. Cheung, W. K. C. & Nguyen, D. X. Lineage factors and differentiation states in lung cancer progression. *Oncogene* **34**, 5771–5780 (2015).
6. Sainz de Aja, J., Dost, A. F. M. & Kim, C. F. Alveolar progenitor cells and the origin of lung cancer. *J. Intern. Med.* **289**, 629–635 (2021).

7. Li, C. & Lu, H. Adenosquamous carcinoma of the lung. *Onco. Targets. Ther.* **Volume 11**, 4829–4835 (2018).
8. Seguin, L., Durandy, M. & Feral, C. C. Lung Adenocarcinoma Tumor Origin: A Guide for Personalized Medicine. *Cancers (Basel).* **14**, 1759 (2022).
9. Moldvay, J. & Tímár, J. KRASG12C mutant lung adenocarcinoma: unique biology, novel therapies and new challenges. *Pathol. Oncol. Res.* **29**, (2024).
10. Dost, A. F. M. *et al.* Organoids Model Transcriptional Hallmarks of Oncogenic KRAS Activation in Lung Epithelial Progenitor Cells. *Cell Stem Cell* **27**, 663-678.e8 (2020).
11. Pantsar, T. The current understanding of KRAS protein structure and dynamics. *Comput. Struct. Biotechnol. J.* **18**, 189–198 (2020).
12. Huang, L., Guo, Z., Wang, F. & Fu, L. KRAS mutation: from undruggable to druggable in cancer. *Signal Transduct. Target. Ther.* **6**, 386 (2021).
13. Tang, Y. *et al.* Targeting KRASG12D mutation in non-small cell lung cancer: molecular mechanisms and therapeutic potential. *Cancer Gene Ther.* **31**, 961–969 (2024).
14. Mogi, A. & Kuwano, H. TP53 Mutations in Nonsmall Cell Lung Cancer. *Biomed Res. Int.* **2011**, (2011).
15. Timar, J. & Kashofer, K. Molecular epidemiology and diagnostics of KRAS mutations in human cancer. *Cancer Metastasis Rev.* **39**, 1029–1038 (2020).
16. Aubrey, B. J., Kelly, G. L., Janic, A., Herold, M. J. & Strasser, A. How does p53 induce apoptosis and how does this relate to p53-mediated tumour suppression? *Cell Death Differ.* **25**, 104–113 (2018).
17. Gross, A., Jockel, J., Wei, M. C. & Korsmeyer, S. J. Enforced dimerization of BAX results in its translocation, mitochondrial dysfunction and apoptosis. *EMBO J.* **17**, 3878–3885 (1998).
18. Shtutman, M., Chang, B.-D., Schools, G. P. & Broude, E. V. Cellular Model of p21-Induced Senescence. in 31–39 (2017). doi:10.1007/978-1-4939-6670-7_3.
19. Sutherland, K. D. *et al.* Multiple cells-of-origin of mutant K-Ras–induced mouse lung adenocarcinoma. *Proc. Natl. Acad. Sci.* **111**, 4952–4957 (2014).
20. Kim, C. F. B. *et al.* Identification of Bronchioalveolar Stem Cells in Normal Lung and Lung Cancer. *Cell* **121**, 823–835 (2005).
21. Jackson, E. L. *et al.* Analysis of lung tumor initiation and progression using conditional expression of oncogenic K-ras. *Genes Dev.* **15**, 3243–3248 (2001).
22. Jackson, E. L. *et al.* The Differential Effects of Mutant p53 Alleles on Advanced Murine Lung Cancer. *Cancer Res.* **65**, 10280–10288 (2005).
23. Heyer, J., Kwong, L. N., Lowe, S. W. & Chin, L. Non-germline genetically engineered mouse models for translational cancer research. *Nat. Rev. Cancer* **10**, 470–480 (2010).
24. Ireson, C. R., Alavijeh, M. S., Palmer, A. M., Fowler, E. R. & Jones, H. J. The role of mouse tumour models in the discovery and development of anticancer drugs. *Br. J. Cancer* **121**, 101–108 (2019).
25. Jung, J., Seol, H. S. & Chang, S. The Generation and Application of Patient-Derived Xenograft Model for Cancer Research. *Cancer Res. Treat.* **50**, 1–10 (2018).
26. Kopper, O. *et al.* An organoid platform for ovarian cancer captures intra- and interpatient heterogeneity. *Nat. Med.* **25**, 838–849 (2019).
27. Sato, T. *et al.* Long-term Expansion of Epithelial Organoids From Human Colon, Adenoma, Adenocarcinoma, and Barrett's Epithelium. *Gastroenterology* **141**, 1762–1772 (2011).
28. Kim, M. *et al.* Patient-derived lung cancer organoids as in vitro cancer models for

therapeutic screening. *Nat. Commun.* **10**, 3991 (2019).
29. Li, Y. F. *et al.* Patient-derived organoids of non-small cells lung cancer and their application for drug screening. *Neoplasma* **67**, 430–437 (2020).
30. Sachs, N. *et al.* Long-term expanding human airway organoids for disease modeling. *EMBO J.* **38**, (2019).
31. Shi, R. *et al.* Organoid Cultures as Preclinical Models of Non–Small Cell Lung Cancer. *Clin. Cancer Res.* **26**, 1162–1174 (2020).
32. Dayton, T. L. *et al.* Druggable growth dependencies and tumor evolution analysis in patient-derived organoids of neuroendocrine neoplasms from multiple body sites. *Cancer Cell* **41**, 2083-2099.e9 (2023).
33. Vazquez-Armendariz, A. I. & Tata, P. R. Recent advances in lung organoid development and applications in disease modeling. *J. Clin. Invest.* **133**, (2023).
34. Vazquez-Armendariz, A. I. *et al.* Multilineage murine stem cells generate complex organoids to model distal lung development and disease. *EMBO J.* **39**, e103476 (2020).
35. Rodríguez-Colman, M. J. *et al.* Interplay between metabolic identities in the intestinal crypt supports stem cell function. *Nature* **543**, 424–427 (2017).
36. Rabata, A., Fedr, R., Soucek, K., Hampl, A. & Koledova, Z. 3D Cell Culture Models Demonstrate a Role for FGF and WNT Signaling in Regulation of Lung Epithelial Cell Fate and Morphogenesis. *Front. Cell Dev. Biol.* **8**, (2020).
37. Ewald, J. A., Peters, N., Desotelle, J. A., Hoffmann, F. M. & Jarrard, D. F. A High-Throughput Method to Identify Novel Senescence-Inducing Compounds. *SLAS Discov.* **14**, 853–858 (2009).
38. Serrano, M., Lin, A. W., McCurrach, M. E., Beach, D. & Lowe, S. W. Oncogenic ras Provokes Premature Cell Senescence Associated with Accumulation of p53 and p16INK4a. *Cell* **88**, 593–602 (1997).
39. Lin, A. W. *et al.* Premature senescence involving p53 and p16 is activated in response to constitutive MEK/MAPK mitogenic s. *GENES Dev.* **12**, 3008–3019 (1998).
40. Downward, J. Ras signalling and apoptosis. *Curr. Opin. Genet. Dev.* **8**, 49–54 (1998).
41. Wong, K. Y. *et al.* Cancer-associated fibroblasts in nonsmall cell lung cancer: From molecular mechanisms to clinical implications. *Int. J. Cancer* **151**, 1195–1215 (2022).
42. Ogawa, H. *et al.* Interleukin-6 blockade attenuates lung cancer tissue construction integrated by cancer stem cells. *Sci. Rep.* **7**, 12317 (2017).
43. Horie, M. *et al.* Differential knockdown of TGF-β ligands in a three-dimensional co-culture tumor- stromal interaction model of lung cancer. *BMC Cancer* **14**, 580 (2014).
44. Browaeys, R., Saelens, W. & Saeys, Y. NicheNet: modeling intercellular communication by linking ligands to target genes. *Nat. Methods* **17**, 159–162 (2020).
45. Galbraith, A. R. *et al.* Chemoprevention of Lung Carcinogenesis by Dietary Nicotinamide and Inhaled Budesonide. *Cancer Prev. Res.* **12**, 69–78 (2019).
46. Breau, M. *et al.* The antioxidant N-acetylcysteine protects from lung emphysema but induces lung adenocarcinoma in mice. *JCI Insight* **4**, (2019).
47. Sayin, V. I. *et al.* Antioxidants Accelerate Lung Cancer Progression in Mice. *Sci. Transl. Med.* **6**, (2014).
48. Nakamura, N., Miyagi, E., Murata, S., Kawaoi, A. & Katoh, R. Expression of Thyroid Transcription Factor-1 in Normal and Neoplastic Lung Tissues. *Mod. Pathol.* **15**, 1058–1067 (2002).
49. Naranjo, S. *et al.* Modeling diverse genetic subtypes of lung adenocarcinoma with a next-generation alveolar type 2 organoid platform. *Genes Dev.* **36**, 936–949 (2022).

## Generative AI statement

AI was used in the report to check the writing for clarity and grammar. This was done following the Generative AI guidelines to make sure the content is clear and correct.

## Supplementary

### Table S1 Media optimization

| Healthy lung media | KP organoid media | MB | MD | MJ | MM |
|---|---|---|---|---|---|
| Advanced DMEM/F12 | Advanced DMEM/F12 | Advanced DMEM/F12 | Advanced DMEM/F12 | DMEM/F12 | Advanced DMEM/F12 |
| Gutamax | Pen/Strep | Glutamax | Glutamax | Pen/Strep | Gutamax |
| Hepes | Glutamax | Hepes | Hepes | Hydrocortisone | Hepes |
| Pen/Strep | Hepes | Pen/Strep | Pen/Strep | ITS | Pen/Strep |
| Noggin | Primocin | | Noggin | FBS | Noggin |
| Rspondin-3 | N-acetylcysteine | | Rspondin-3 | | ITS |
| B27 | Y-27632 | | B27 | | N-acetyltcysteine |
| Nicotinamide | ITS | | Nicotinamide | | Primocin |
| N-acetylcysteine | Noggin | | N-acetylcysteine | | Y-27632 |
| Primocin | Nicotinamide | | Primocin | | Nicotinamide |
| Y-27632 | | | Y-27632 | | |
| A83-01 | | | A83-01 | | |
| SB202190 | | | SB202190 | | |
| FGF7 | | | FGF7 | | |
| FGF10 | | | FGF10 | | |

| M1 | M2 | M3 | M4 | M5 | M6 |
|---|---|---|---|---|---|
| Advanced DMEM/F12 | Advanced DMEM/F12 | Advanced DMEM/F12 | Advanced DMEM/F12 | Advanced DMEM/F12 | Advanced DMEM/F12 |
| Gutamax | Gutamax | Gutamax | Gutamax | Gutamax | Gutamax |
| Hepes | Hepes | Hepes | Hepes | Hepes | Hepes |
| Pen/Strep | Pen/Strep | Pen/Strep | Pen/Strep | Pen/Strep | Pen/Strep |
| Noggin | Noggin | Nicotinamide | Nicotinamide | Nicotinamide | Nicotinamide |
| N-acetyltcysteine | N-acetyltcysteine | N-acetyltcysteine | Noggin | Noggin | Noggin |
| Primocin | Primocin | Primocin | Primocin | N-acetyltcysteine | Primocin |
| Y-27632 | Y-27632 | Y-27632 | Y-27632 | Y-27632 | N-acetyltcysteine |
| Nicotinamide | ITS | ITS | ITS | ITS | ITS |

| M7 | M8 | M9 | M10 | M11 | M12 | M13 |
|---|---|---|---|---|---|---|
| Advanced DMEM/F12 | Advanced DMEM/F12 | Advanced DMEM/F12 | Advanced DMEM/F12 | Advanced DMEM/F12 | Advanced DMEM/F12 | Advanced DMEM/F12 |
| Gutamax | Gutamax | Gutamax | Gutamax | Gutamax | Gutamax | Gutamax |
| Hepes | Hepes | Hepes | Hepes | Hepes | Hepes | Hepes |
| Pen/Strep | Pen/Strep | Pen/Strep | Pen/Strep | Pen/Strep | Pen/Strep | Pen/Strep |
| B27 | Nicotinamide | Noggin | N-acetylcysteine | Primocin | Y-27632 | ITS |

| M14 | M15 | M16 | M17 | M18 | M19 | M20 |
|---|---|---|---|---|---|---|
| Advanced DMEM/F12 | Advanced DMEM/F12 | Advanced DMEM/F12 | Advanced DMEM/F12 | Advanced DMEM/F12 | Advanced DMEM/F12 | Advanced DMEM/F12 |
| Gutamax | Gutamax | Gutamax | Gutamax | Gutamax | Gutamax | Gutamax |
| Hepes | Hepes | Hepes | Hepes | Hepes | Hepes | Hepes |
| Pen/Strep | Pen/Strep | Pen/Strep | Pen/Strep | Pen/Strep | Pen/Strep | Pen/Strep |
| A83-01 | SB202190 | FGF7 | FGF10 | Rspondin-3 | CHIR99021 | EGF |

| B27 | ITS |
|---|---|
| Advanced DMEM/F12 | Advanced DMEM/F12 |
| Gutamax | Gutamax |
| Hepes | Hepes |
| Pen/Strep | Pen/Strep |
| Noggin | Noggin |
| Rspondin-3 | Rspondin-3 |
| B27 | ITS |
| Nicotinamide | Nicotinamide |
| N-acetylcysteine | N-acetylcysteine |
| Primocin | Primocin |
| Y-27632 | Y-27632 |
| A83-01 | A83-01 |
| SB202190 | SB202190 |
| FGF7 | FGF7 |
| FGF10 | FGF10 |

## Table S2. Reagents

| Ragent | Source | Identifier |
|---|---|---|
| **Antibodies** | | |
| Anti-TTF1 antibody [EP1584Y] (NKX2-1) | Abcam | ab76013 |
| p53 Antibody (DO-1) | SCBT | sc-126 |
| Donkey anti-Rabbit IgG (H+L) Highly Cross-Adsorbed Secondary Antibody, Alexa Fluor™ Plus 488 | Thermo - Invitrogen | A32790 |
| Donkey anti-Mouse IgG (H+L) Highly Cross-Adsorbed Secondary Antibody, Alexa Fluor™ Plus 555 | Thermo - Invitrogen | A32773 |
| **Chemicals, peptides, and recombinant proteins** | | |
| Cultrex Basement Membrane Extract (BME), Growth Factor Reduced, Type 2 | R&D Systems, Bio-Techne | 3533-010-02 |
| TrypLE Express Enzyme (13), phenol red | Thermo Fisher Scientific | Cat#12605028 |
| Advanced DMEM/F12 | Gibco | 12634028 |
| DMEM/F12 | Fisher scientific | 11320033 |
| Glutamax 100x | Gibco | 11574466 |
| Pen-Strep | Thermo Fisher Scientific | Cat#15140122 |
| HEPES | Gibco | 11560496 |
| Noggin | ImmunoPrecise Antibodies | N002 - 100ml |
| R-spondin-3 | ImmunoPrecise Antibodies | R001 - 100ml |
| B27 (minus VitA) | Gibco | 15440584 |
| Insulin Transferrin Selenium | Fisher scientific | 15383661 |
| Nicotinamide | MERCK (Sigma) | N0636-100G |
| N-acetyl cysteine | MERCK (Sigma) | A9165-25G |
| Primocin | Invivogen | Cat#ANT-PM-2 |
| Y-27632 | Abmole | M1817 - 10 mg |
| A83-01 | Bio-Techne | 2939-10mg |
| SB 202190 | Sigma Aldrich | S7076-5MG |
| FGF7 | Peprotech | 100-19 250 ug |
| FGF10 | Peprotech | 100-26 1 mg |
| Wnt surrogate | ImmunoPrecise Antibodies | N001 - 100µg |
| Fetal Bovine Serum | Thermo Fisher Scientific | A5256701 |
| Hydrocortisone | | |
| EGF | Peprotech | AF-100-15 |
| CHIR | Bio-Techne | 4423 |
| Alexa Fluor™ 647 Phalloidin | Thermo - Invitrogen | A22287 |
| DNAse I | Sigma | DN25-100mg |
| Red blood cell lysis buffer | Sigma | 11814389001 |
| Collagenase | MERCK (Sigma) | C9407-500MG |
| NcoI-HF Restriction Enzyme | NEB | R3193L |
| BamHI-HF Restriction Enzyme | NEB | R3136L |
| Agarose low EEO | SigmaAldrich | A9539-500G |
| SybrSafe gel staining dye | ThermoFischer | S33102 |
| Nutlin | Medchemexpress | HY-10029 |
| **Kits** | | |
| EndoFree Plasmid Maxi Kit (10) | Qiagen | 12362 |
| GeneJET Gel Extraction Kit | Thermo Fisher Scientific | 2919786 |
| GeneArt Gibson Assembly HiFi Cloning Kit | Thermo Fisher Scientific | A46629 |
| Stbl3 competent cells | FisherScientific | 10193952 |

## Table S3. Media components and concentrations

| Media reagent | Final concentration |
|---|---|
| Glutamax (100x) | 1X |
| Pen-Strep | 10 mM |
| HEPES | 10 mM |
| Noggin UPE | 1% |
| R-spondin-3 UPE | 1% |
| B27 (minus VitA) (50X) | 1X |
| Insulin Transferrin Selenium (100X) | 1X |
| Nicotinamide | 5 mM |
| N-acetyl cysteine | 1.25 mM |
| Primocin | 10 mM |
| Y-27632 | 2.5 uM |
| A83-01 | 500 nM |
| SB 202190 | 3 uM |
| FGF7 | 25 ng/mL |
| FGF10 | 100 ng/mL |
| Wnt surrogate | 16.4 nM |
| Fetal Bovine Serum | 10% |
| Hydrocortisone | 4 ug/mL |
| EGF | 50 ng/mL |
| CHIR | 3uM |

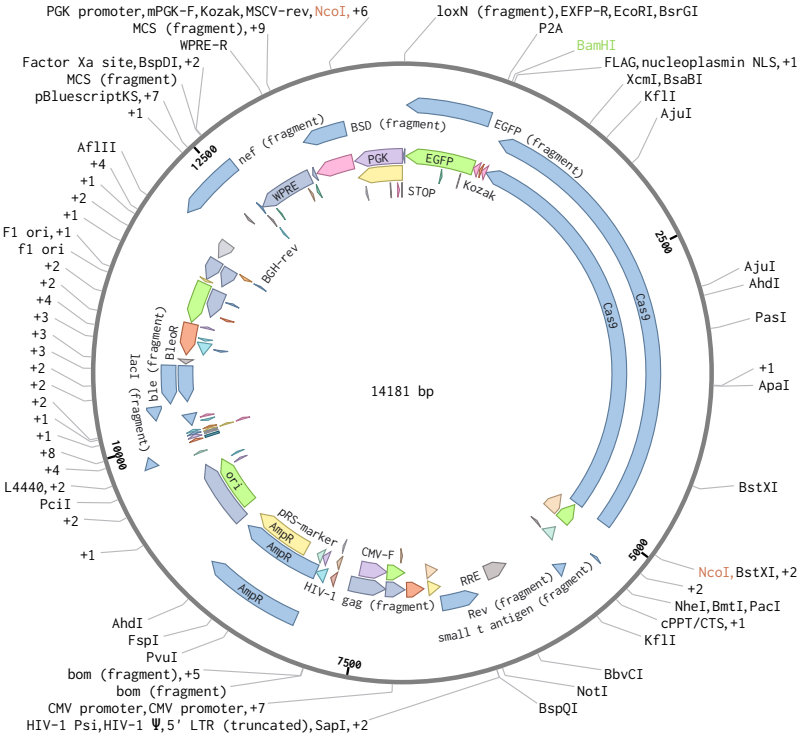


***Figure S1 Plasmid map of the backbone plasmid.*** *Key elements include the EF1a promoter, the Cas9 gene, the 2A spacer, and the EGFP gene. Restriction sites for NcoI and BamHI are shown for cloning purposes.*

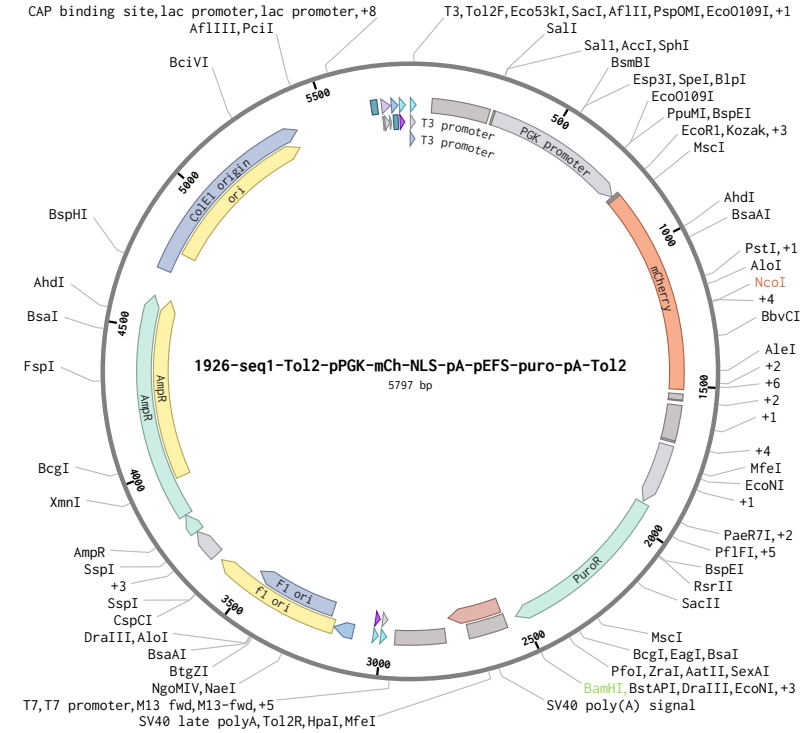


***Figure S2 Plasmid map of the insert plasmid.*** *Key elements include the EF1a promoter and the Puromycin resistance gene for puromycin selection. Restriction sites for NcoI and BamHI are shown for cloning purposes.*

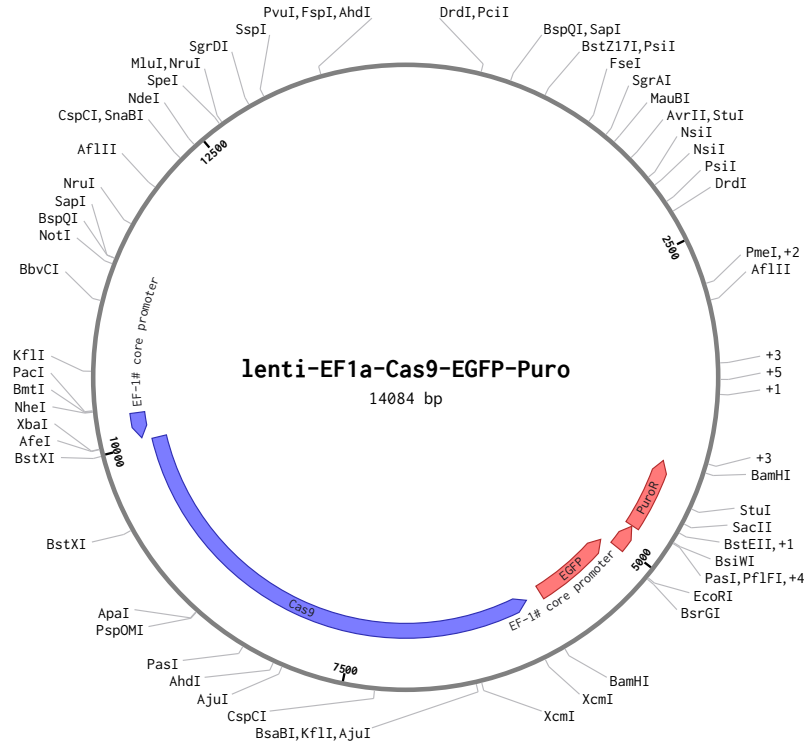


***Figure S3 Plasmid map of the final plasmid.*** *Plasmid contains the EF1a core promotor followed by the Cas9 gene driving expression of the EGFP gene. The plasmid contains the inserted EF1a promotor driving expression of the Puromycin resistance gene.*

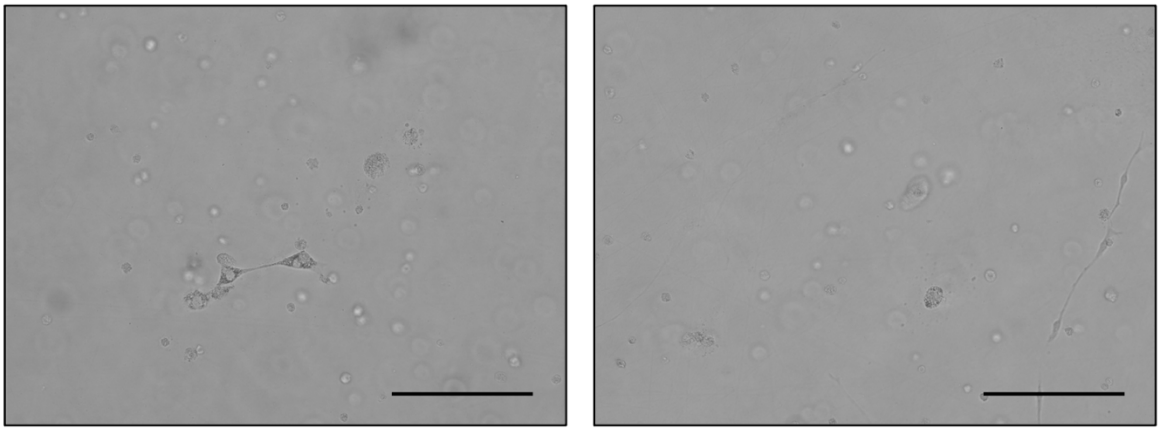

***Figure S4 Dark colonie formation of Kmut cells*** *Two representative brightfield microscopy images of Kmut 3D cell cultures showing darker colony morphologies .Scale bar represents 150 µm*

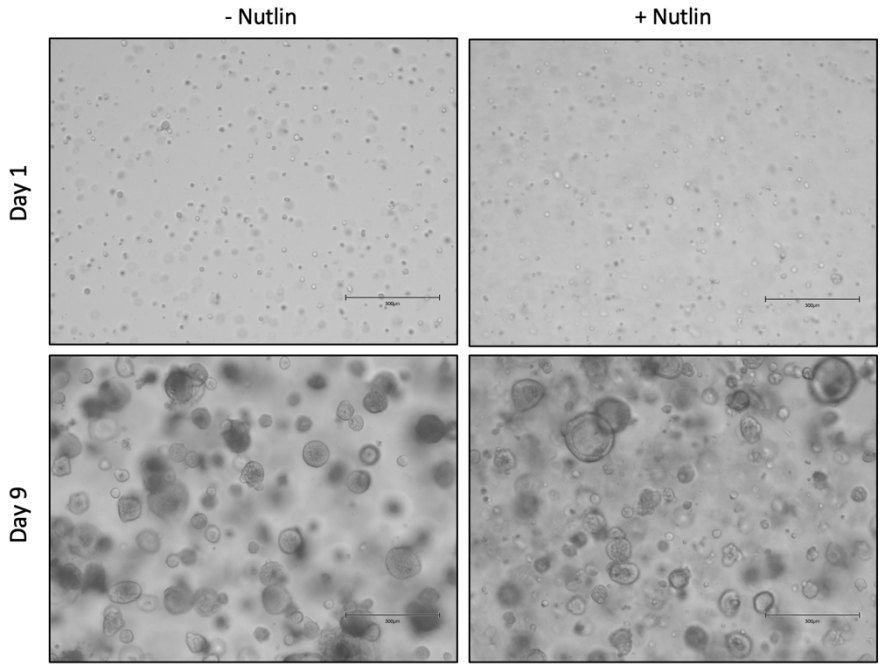


***Figure S5 KP92 organoid formation with and without Nutlin.*** *KP92 organoids cultured in the presence (+Nutlin) and absence (-Nutlin) of 10 uM Nutlin were observed on Day 1 and Day 9. Minimal differences in organoid formation are seen on Day 1, while by Day 9, larger and more numerous organoids are visible in both conditions. Scale bars represent 200 µm.*